ARTICLE

From Graphene to Metal Oxide Nanolamellas: A Phenomenon of Morphology Transmission

Sheng Chen, Junwu Zhu, and Xin Wang*

Key Laboratory for Soft Chemistry and Functional Materials (Nanjing University of Science and Technology), Ministry of Education, Nanjing 210094, China

ABSTRACT Single-layer-graphene and few-layer-graphene structures have been predicted to have high specific surface area. Recent research has focused largely on utilizing the intriguing morphology of graphene as building blocks or substrates, keeping the structure undisturbed. Relatively little attention has been paid to explore the framework substitution of graphene. Here, we report a procedure for morphology transmission from graphene to metal oxide nanolamellas by *in situ* replacement with the framework of graphene. Our approach involves using graphene sheets as the starting reagent, thereby transmitting the morphology of layered structure from graphene to as-prepared metal oxides. The heteroconfiguration of as-prepared MnO_2 could play a role in preventing microstructure degradation in the electrochemical cycling process, bestowing MnO_2 nanolamellas an excellent electrochemical stability as a supercapacitor electrode. It is worth mentioning that this methodology is readily adaptable to fabricating MnO_2, Co_3O_4, and Cr_2O_3 nanowires from single-walled carbon nanotubes and Co_3O_4 and Cr_2O_3 nanolamellas from graphene sheets.

KEYWORDS: graphene · metal oxide · nanolamellas · morphology transmission · electrochemical behavior

As a rising star, graphene has triggered an exciting new area in the field of carbon nanoscience with ever-increasing scientific and technological impetus.[1,2] The novel electronic performances of graphene have been observed;[3,4] the charge carriers behave as massless Dirac fermions,[5] and unique properties such as a remarkable thermal conductivity,[6] an ambipolar field effect,[3] and a room-temperature quantum Hall effect[7] have all been well documented. Some techniques, such as liquid-phase exfoliation of graphite,[8,9] chemical vapor deposition,[10] the self-assembly approach,[11,12] and chemical reduction of graphite oxide,[13,14] have all taken us a step closer to processing graphene sheets in bulk quantities. As an unrolled carbon nanotube, graphene has been a hot topic as a superior platform for building nanocomposites.[15,16]

Currently, the main interests in graphene are centered on two aspects: pursuing for feasible approaches to produce graphene sheets and further exploring peculiar properties of individual graphene nanosheets or graphene-based nanocomposites. In these works, the basic framework of graphene remains unchanged. Relatively little attention has been paid so far to explore the framework substitution of graphene. Taking into account that graphene is a 2-dimensional network of carbon atoms, it can be oxidized with some oxidizing reagents, such as $KMnO_4$, $K_2Cr_2O_7$, Na_2CrO_4, $Co(NO_3)_2 \cdot 6H_2O$, *etc.*, yielding corresponding metal oxide materials by means of sacrificing graphene itself. Thereby, this method may open a promising avenue for replacing the framework carbon atoms of graphene. On the other hand, in view of the unique layered structure and exceptional physicochemical properties of these intriguing materials, there may be some distinctive characters of the as-prepared products.

MnO_2 is known as a promising electrode material for applications in supercapacitors and has raised much interest because of its environmental compatibility, low cost, and abundant availability on the earth.[16] However, the MnO_2 material obtained from the traditional coprecipitation method has a low specific capacitance owing to its low specific surface area.[19] Moreover, although nanoscale MnO_2 particles possess large surface area and relatively high specific capacitance, the microstructure is easily damaged during electrochemical cycling, giving a relatively poor electrochemical stability.[19]

To extend the application of graphene, here we report a general procedure to prepare nanoscale metal oxides by *in situ* replacement of carbon atoms in the graphene framework and also demonstrate, for the first time, that MnO_2, Co_3O_4, and Cr_2O_3 with

*Address correspondence to wxin@public1.ptt.js.cn.

Received for review July 31, 2010 and accepted September 1, 2010.

Published online September 9, 2010. 10.1021/nn101857y

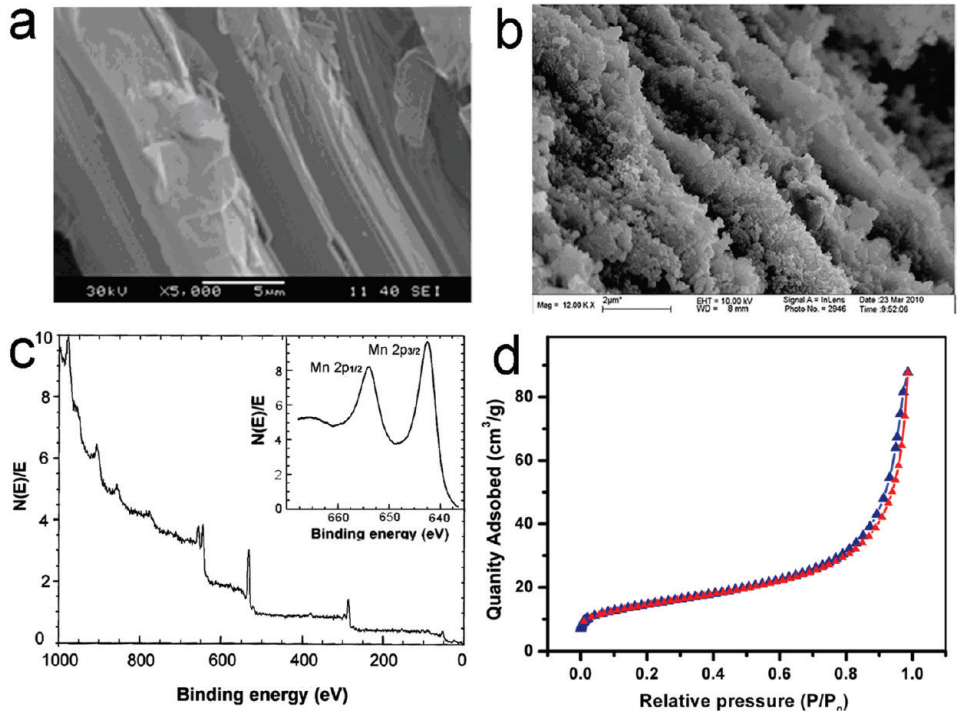

Figure 1. (a) FESEM images of graphene sheets; (b) FESEM, (c) XPS, and (d) nitrogen adsorption/desorption isotherm of the as-obtained MnO_2-lamellas. The inset of panel c is Mn (2P) peaks of MnO_2 nanolamellas in XPS analyses.

nanolamella structure have been dramatically obtained, presenting a new application of graphene. To the best of our knowledge, there has been little research concerning this field so far. In our approach, the as-obtained MnO_2 product has exhibited a large surface area and excellent electrochemical properties in neutral electrolyte, displaying satisfactory specific capacitance and high electrochemical stability. Notably, as a single-walled carbon nanotube (SWNT) can be considered as a rolled up graphene sheet, this methodology consequently is readily adaptable to fabricating MnO_2, Co_3O_4, and Cr_2O_3 nanowires from SWNTs. This method would be appropriate for a process to be scaled up for bulk scale production in nanotechnology.

RESULTS AND DISCUSSION

Being a starting material, graphene was produced by dispersion and exfoliation of bulk graphite in *N*-methylpyrrolidone (see Methods). Field emission scanning electron microscopy (FESEM), transmission electron microscopy (TEM), and Raman analyses verify the exfoliation of bulk graphite to graphene sheets (Figure 1S, Supporting Information).[8] The representative method involves using graphene sheets as starting material in conjunction with $KMnO_4$ to prepare MnO_2 material in a dual-solvent system and hence transmitting the unique layered structure of graphene to MnO_2.

The definitive evidence that almost all the carbon atoms of graphene can be replaced by MnO_2 to form nanolamellas was obtained with FESEM (Figure 1a,b) and TEM (Figure 2S a,b, Supporting Information) analyses. It can be seen that the lamellar structure of graphene was indeed transmitted to the products. The brinks of the sheets can be clearly discerned; the lamellar structures of the products are fully seen. Moreover, it seems that these lamellas are constituted by many nanoscale particles, suggesting the *in situ* growth of MnO_2 from the carbon atoms of graphene.

The MnO_2 lamellas were further examined by X-ray photoemission spectroscopy (XPS, Figure 1c), UV−vis (see Supporting Information, Figure 2Sd), Raman spectroscopy (Figure 2c), surface area measurements (Figure 1d), and thermo-gravimetric analysis (TGA, Figure 2Sc, Supporting Information). The average oxidation state (AOS) of Mn was determined by a two-step titration method (see Methods).

XPS results indicate that the product contains Mn and O as the main components, while C and K are impurities. The peaks of Mn $2p_{3/2}$ and $2p_{1/2}$ which are centered at 642.4 and 654.2 eV, respectively, with a spin-energy separation of 11.8 eV are in agreement with reported data of Mn $2p_{3/2}$ and Mn $2p_{1/2}$ in MnO_2. The average oxidation state of manganese, as determined by the two-step titration, is 3.87 with MnO_2 making up 90.1% of the total products by mass. Additionally, a broad absorption centered at around 360 nm corresponding to d−d transitions of Mn ions in MnO_2 nanocrystals[17,18] is observed in UV−vis spectroscopy; the characteristic Raman peak at around 640 cm^{-1} corresponds to Mn−O vibrations perpendicular to the direction of the MnO_6 octahedral double chains of MnO_2. All of these sets of data are in conformity with each

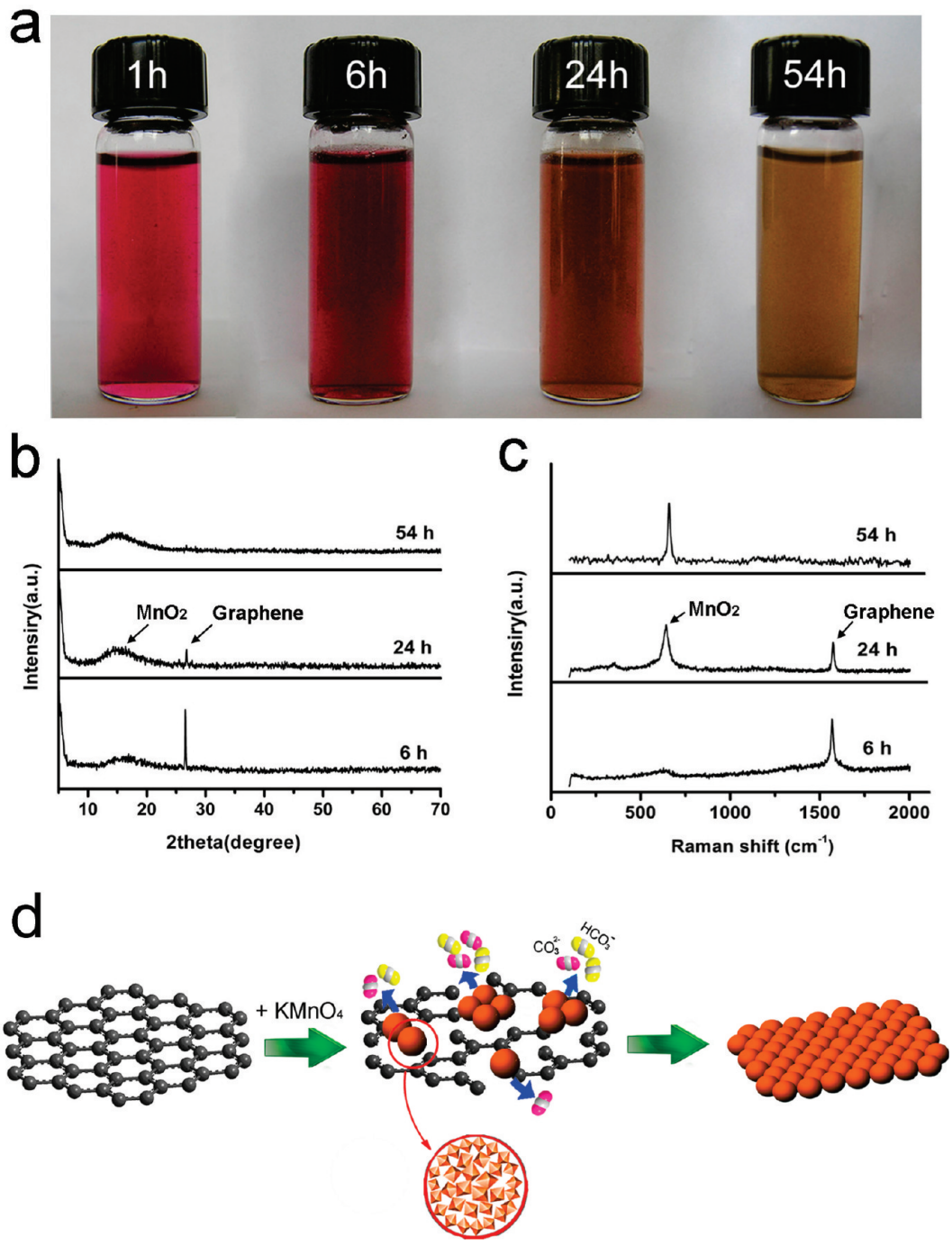

Figure 2. (a) Digital pictures of the reacting solution from 1 to 54 h (note: 1 mL of reacting mixture was diluted with 4 mL of DI-water for reliable comparison); (b) XRD and (c) Raman analyses of the samples taken at different time intervals; (d) illustrations for the formation process of MnO_2 nanolamellas from graphene.

other, providing evidence that MnO_2 material was obtained.

Surface area measurements indicate that the MnO_2 nanolamellas have a Brunauer−Emmett−Teller (BET, nitrogen, 77 K) surface area of 50.3 $m^2 \cdot g^{-1}$, with pore volume of 0.135 $cm^2 \cdot g^{-1}$, and BJH desorption average pore diameter of 14.4 nm. Remarkably, this value is much higher than the MnO_2 produced by traditional co-precipitation of $KMnO_4$ and Mn^{2+}.[19] A large surface area suggests wider utilization of the as-prepared material.

In the TGA curve (see Supporting Information, Figure S2c) a 15.2% weight loss from 80 to 500 °C resulting from the dehydration of the adsorbed water and the lattice water is observed. At higher temperatures a 10.6% weight loss may be attributed to the transformation of MnO_2 into Mn_2O_3[17,18] and the burning of the residual carbon in air.

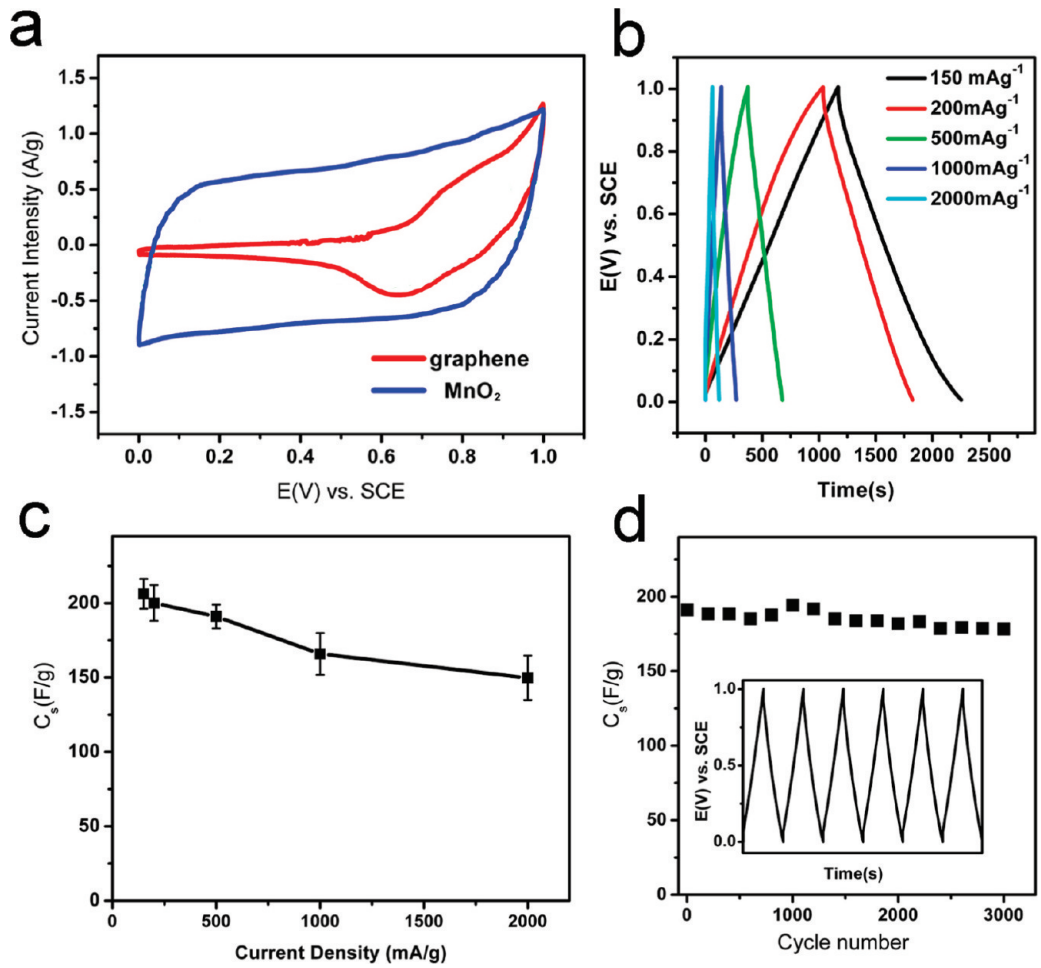

Figure 3. (a) CV plots of graphene and MnO_2 at 5 mV · s^{-1}; (b) galvanostatic charge/discharge measurements of MnO_2 nanolamellas at different current densities; (c) plot of specific capacitance (C_s) as a function of current density of MnO_2 lamellas; (d) cycle life of MnO_2 lamellas at 500 mA · g^{-1}.

Moreover, the *in situ* replacement process of graphene by MnO_2 was further investigated by taking samples for testing from the reaction mixture at different time intervals. Figure 2a shows the pictures of the reaction system from 1 to 54 h. For a better distinction, 1 mL of reacting mixture was diluted with 4 mL of DI-water. The solution color gradually turned from purple to golden brown. No further noticeable color change was observed after 54 h (*e.g.*, 72 h, Figure 3S, Supporting Information), suggesting the completion of the reaction after that period. In Figure 2b,c, the increasing peak intensity ratio of MnO_2/graphene in both XRD and Raman spectra from 6 to 24 h provides evidence for yielding MnO_2 with the depletion of graphene sheets. It can be seen from the TEM and FESEM results in Figure 4S (Supporting Information) that the graphene sheets were corroded while a few nanoscale particles formed on the surface and edges at 24 h, implying the growth of MnO_2 at

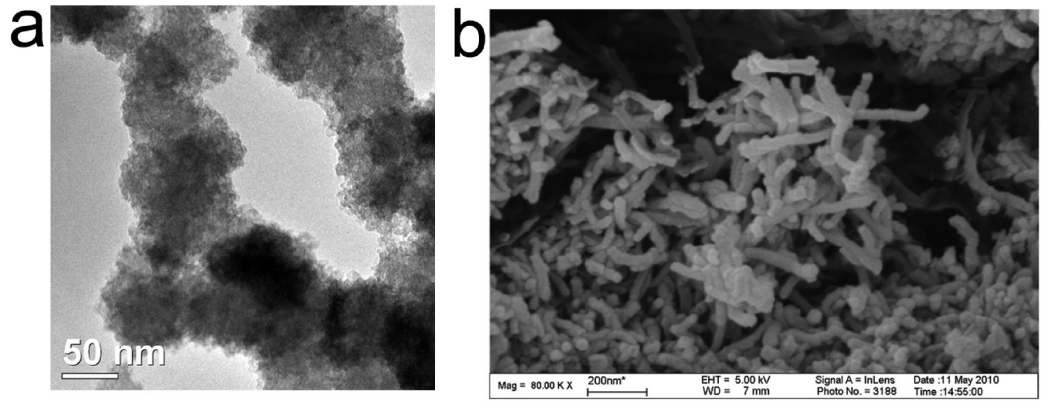

Figure 4. (a)TEM and (b) FESEM images of the as-prepared MnO_2 nanowires from SWNTs.

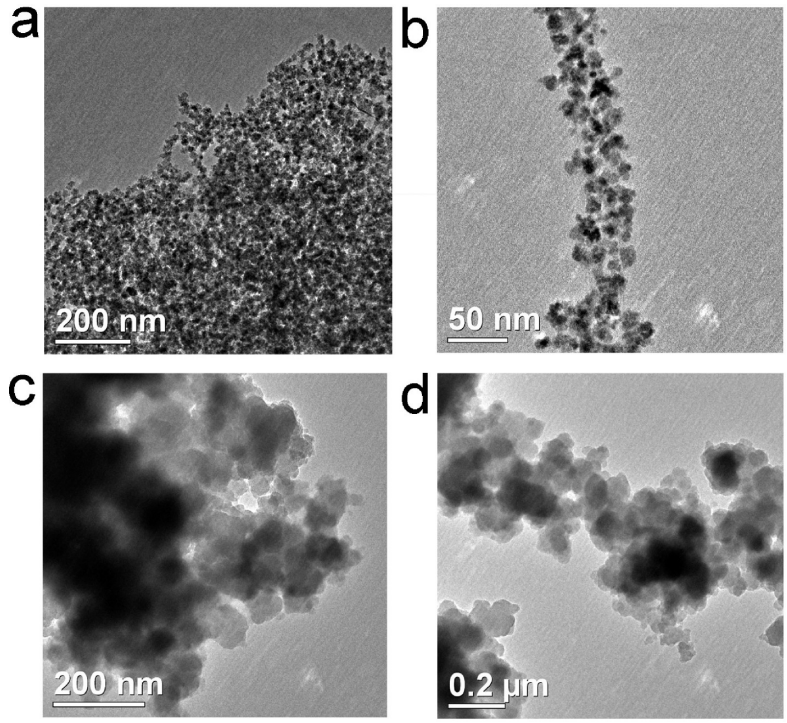

Figure 5. TEM images of the as-prepared Co_3O_4 (a) nanolamellas (b) and nanowires, and chromium oxide (c) nanolamellas and (d) nanowires.

the cost of the carbon atoms of graphene. Moreover, it was found during the whole process that the solution pH value was increasing with the reaction, probably as a result of the formation of CO_3^{2-} or HCO_3^-. The reaction was much faster upon heating, but only the results obtained at ambient temperature are presented.

The whole process is illustrated in Figure 2d. Generally, graphene exhibits a lamellar structure. With the introduction of $KMnO_4$ aqueous solution into the graphene dispersion system, carbon atoms of graphene can react with $KMnO_4$ in a water-containing system.[20] In view of the phenomena above, the whole process is assumed to be: $4KMnO_4 + 3C + H_2O \rightarrow 4MnO_2 + K_2CO_3 + 2KHCO_3$. Therefore, elimination of the carbon atoms of graphene could lead to the *in situ* formation of MnO_2 nanoparticles. Almost all the carbon atoms of graphene were replaced by MnO_2 molecules, and interestingly the lamellar structure of graphene was transmitted to the as-formed MnO_2.

The as-prepared products were fabricated to electrodes and tested using cyclic voltametry (CV) and galvanostatic charge/discharge measurements in 1 M Na_2SO_4 aqueous electrolyte (Figure 3). The rectangular and symmetric CV curves of MnO_2 nanolamellas in Figure 3a indicate the ideal pseudocapacitive nature of the as-fabricated electrode, while the lack of symmetry in graphene can be attributed to its double-layer capacitance in neutral electrolyte.

Specific capacitance of MnO_2 calculated at 150, 200, 500, 1000, and 2000 $mA \cdot g^{-1}$ from the discharge curves is 206.2, 200.1, 191.0, 165.8, and 149.7 $F \cdot g^{-1}$, respectively (Figure 3b,c).[21] About 72.6% specific capacitance was retained even with the current density increasing from 150 to 2000 $mA \cdot g^{-1}$. Consistently good performance of MnO_2 nanolamellas over a wide range of current densities suggests this material is promising as supercapacitor electrodes. Additionally, when the charge−discharge was cycled at 500 $mA \cdot g^{-1}$, as shown in Figure 3d, there is only a slight decrease in capacitance of less than 10% even after 3000 cycles, demonstrating a great stability.

Of note is that the electrochemical properties of the as-prepared MnO_2 nanolamellas are more competitive than MnO_2 with many other morphologies, such as flowers (168 $F \cdot g^{-1}$),[22] hollow urchins (147 $F \cdot g^{-1}$),[23] clews (120 $F \cdot g^{-1}$),[24] and (2 × 4) tunnel nanorods (140 $F \cdot g^{-1}$).[25] This distinctive structure (large surface area, pore volume, and average pore diameter) is documented to contribute to the insertion−deinsertion of ions from electrolyte to electrode, giving it good electrochemical performances.[19] Moreover, in our previous report, when graphene oxide served as the platform and MnO_2 as the building blocks, the specific capacitance of the product at 500 $mA \cdot g^{-1}$ was only 141.5 $F \cdot g^{-1}$ with a decrease of 15.9% after 1000 cycles,[16] obviously less competitive than that of MnO_2 nanolamellas. Furthermore, although the nanoscale MnO_2 synthesized from the typical microemulsion route has a larger BET surface area (123.39 $m^2 \cdot g^{-1}$, while that of the MnO_2 nanolamellas is 50.3 $m^2 \cdot g^{-1}$), only less than 80% of the initial specific capacitance was retained after 500 cycles.[19] Recent studies show that the decrease in specific capacitance is attributed to the corrosion behavior

and degradation of the MnO_2 microstructure.[19] In our procedure, the MnO_2 nanolamellas have more stable and less corrodible microstructure as compared with that of nanoscale-particle counterpart in electrochemical tests. Therefore, this unique layered structure bestows MnO_2 material with an excellent electrochemical stability. Good electrochemical properties of the as-prepared MnO_2 nanolamellas suggest they are promising candidates as electrode materials for supercapacitors.

It is worth mentioning that this methodology is readily adaptable to fabricating MnO_2 nanowires from single-walled carbon nanotubes. Controlled experiments using SWNTs and $KMnO_4$ as the precursors *via* a similar procedure were carried out (see Methods). Representative TEM and FESEM images of the as-obtained products are displayed in Figure 4. It is clearly seen that the MnO_2 products show nanowire morphology with diameters of about 50 nm and lengths of a few hundred nanometers. Similarly, the linear shape of SWNTs was transmitted to MnO_2. Moreover, as is shown in Figure 5, our methodology is also adaptable to $Co(NO_3)_2 \cdot 6H_2O$ and Na_2CrO_4, producing the Co_3O_4 and Cr_2O_3 nanolamellas and nanowires. It is expected that the easy synthesis of these unique nanostructures will endow those materials with more intriguing applications in catalysis, Li-batteries, dyes, *etc*.

CONCLUSIONS

Collectively, a general procedure by *in situ* substitution of the framework of graphene to produce metal oxide nanolamellas has been reported by our group. The study of the growth mechanism of the manganese oxide nanolamellas and nanowires is still currently under way. It should be mentioned that we have pushed the potential utilization of graphene to a broader horizon, which is believed to be of great significance from both a scientific and technological point of view. We have provided evidence to verify that graphene is not just a common union of carbon atoms, but rather, it is unique, having valuable properties and diverse potential applications.

METHODS

Synthesis. Natural flake graphite with an average particle size of 45 μm (99%) was purchased from Qingdao Zhongtian Company (Qingdao, China). Graphene sheets were produced by dispersion and exfoliation of bulk graphite in NMP at a starting concentration of 0.1 mg/mL according to the report of Colman *et al*.[8] The as-obtained graphene dispersion (100 mL) was vigorously stirred, while 5 mL of $KMnO_4$ solution (80 mg of $KMnO_4$ dissolved in 5 mL of deionized water) was introduced rapidly. The mixture was kept standing in a covered beaker under ambient conditions until the purple color turned to a golden brown. This process lasted 2−3 days. During and after the reaction, no obvious precipitation occurred. The as-generated product was finally centrifuged and washed with DI-water and ethanol, respectively. The reaction was found to be much faster upon heating, for reliable comparison; however, only the results obtained at ambient temperature are presented here. To prepare Co_3O_4 nanolamellas, $Co(NO_3)_2 \cdot 6H_2O$ (200 mg) were dissolved in 5 mL of deionized water and then introduced into graphene dispersion (100 mL) vigorously stirring. The as-obtained mixture was loaded into a Teflon-lined stainless steel autoclave and heated at 180 °C for 12 h. The autoclave was allowed to cool to room temperature after the dwell time. Then, the powders obtained were collected and washed repeatedly and finally dried. This procedure is also adaptable to chromium oxide nanolamellas when $Co(NO_3)_2 \cdot 6H_2O$ (200 mg) was replaced by Na_2CrO_4 (400 mg).

The synthesis of MnO_2 nanowires from SWNTs was similar to that of MnO_2 nanolamellas except that (1) the starting concentration of SWNTs/NMP solution was 0.04 mg/mL (4 mg of SWNTs dispersed in 100 mL of NMP); (2) 20 mg of $KMnO_4$ was dissolved in 5 mL of deionized water to form a solution. The synthesis of Co_3O_4 and Cr_2O_3 nanowires is similar to their nanolamellas with the graphene dispersion replaced by SWNT dispersion (0.04 mg/mL).

Characterization. Powder X-ray diffraction (XRD) analyses were performed on a Bruker D8 Advance diffractometer with Cu Kα radiation ($\lambda \approx 1.54$ Å). UV−vis absorption spectra were obtained using a Rayleigh UV-1201 (Beijing, China) recording spectrophotometer. Raman spectra were run on a Renishaw Raman microscope. The excitation line at 514.5 nm provided by an argon ion laser was used. Thermogravimetric analyses (TGA) were performed on a TGA/SDTA851e thermogravimetric analyzer from 80 to 800 °C at a heating rate of 20 °C · min^{-1} in air flow. X-ray photoelectron spectra (XPS) were recorded on a Perkin-Elmer PHI5300 X-ray photoelectron spectrometer, using Al Kα ($h\upsilon = 1486.7$ eV) X-ray as the excitation source. Morphologies of as-obtained products were observed on a transmission electron microscope (TEM, JEOL JEM-2100) and field emission scanning electron microscopy (FESEM, LEO-1550). Moreover, the Brunauer−Emmett−Teller (BET) surface area and pore volume were measured by the nitrogen gas adsorption−desorption method at 77 K using a TriStar II 3020 Micrometrics apparatus. The pore size distribution was calculated by the Barrett−Jayner−Halenda (BJH) method using the desorption branch of the isotherm.

Electrochemical Measurement. The electrochemical properties of as-obtained products were investigated under a three-electrode cell configuration at room temperature. The working electrodes were fabricated by mixing the prepared powders with 15 wt % acetylene black and 5 wt % polytetrafluorene-ethylene (PTFE) binder. A small amount of DI-water was added to the mixture to produce a homogeneous paste. The mixture was pressed onto nickel foam current-collectors (1.0 cm ×1.0 cm) to make electrodes. The mass of the active material was in a range of 5.6−15.2 mg. Before the electrochemical test, the prepared electrode was soaked overnight in a 1 M Na_2SO_4 solution. Electrochemical characterization was carried out in a conventional three-electrode cell with 1 M Na_2SO_4 aqueous solution as the electrolyte. Platinum foil and a saturated calomel electrode (SCE) were used as the counter-electrode and reference electrode, respectively. CV measurements were conducted on a CHI 660B electrochemical workstation (Shanghai CH Instrument Company, China). Galvanostatic charge−discharge measurement was performed on a Land Battery workstation at 22 °C (Wuhan Land Instrument Company, China).

Mn Average Oxidation State (AOS) Determination. The AOS was determined using a two-step procedure. For the first step, a total of about 50 mg of product and 0.35 g of $Na_2C_2O_4$ were dispersed in 8 mL of sulfuric acid. The suspension was heated until particles were completely dissolved. Then it was diluted to 30 mL with deioned water and heated to 75−85 °C. The mixture was then titrated with a 0.02 mol · L^{-1} $KMnO_4$ aqueous solution to determine the $Na_2C_2O_4$ excess (with the appearance of the pink color in the solution and did not fade in 30 s). For the second step, the solution was cooled and diluted in an appropriate volumetric flask, where 0.1 g of hydroxylamine hydrochloride, 1−2 mL of triethanolamine, and 5−10 mL of ammonium hydroxide

were introduced. The mixture was titrated with a 0.02 mol · L^{-1} EDTA aqueous solution with eriochrome black T as the indicator until it turned to blue. The possible reactions occurring during this process are as follows:

$$MnO_2 + C_2O_4^{2-} + 4H^+ \rightarrow Mn^{2+} + 2CO_2 + 2H_2O$$

$$5C_2O_4^{2-} + 2MnO_4^- + 16H^+ \rightarrow 2Mn^{2+} + 10CO_2 + 8H_2O$$

$$Mn^{2+} + EDTA \rightarrow Mn(EDTA)^{2+}$$

The AOS and total content of MnO_2 in the products were calculated from the above formulations.

Acknowledgment. This investigation was supported by the Natural Science Foundation of China and China Academy of Engineering Physics (No. 10776014 and 50902070), the Natural Science Foundation of Jiangsu province (No.BK2009391), the Research Fund for the Doctoral Program of Higher Education of China (No. 20093219120011), and NUST Research Funding, No. ZDJH07.

Supporting Information Available: TEM and FESEM, Raman spectroscopy and digital image of exfoliated graphene; TEM, TG, and UV−vis absorption of MnO_2 nanolamellas; digital pictures of the reacting solution at 54 h and 72 h; TEM and FESEM images of the samples taken at 24 h. This material is available free of charge *via* the Internet at http://pubs.acs.org.

REFERENCES AND NOTES

1. Geim, A. K.; Novoselov, K. S. The Rise of Graphene. *Nat. Mater.* **2007**, *6*, 183–191.
2. Geim, A. K. Graphene: Status and Prospects. *Science* **2009**, *324*, 1530–1534.
3. Novoselov, K. S.; Geim, A. K.; Morozov, S. V.; Jiang, D.; Zhang, Y.; Dubonos, S. V.; Grigorieva, I. V.; Firsov, A. A. Electric Field Effect in Atomically Thin Carbon Films. *Science* **2004**, *306*, 666–669.
4. Wu, J.; Pisula, W.; Mullen, K. Graphenes as Potential Material for Electronics. *Chem. Rev.* **2007**, *107*, 718–747.
5. Novoselov, K. S.; Geim, A. K.; Morozov, S. V.; Jiang, D.; Katsnelson, M. I.; Grigorieva, I. V.; Dubonos, S. V.; Firsov, A. A. Two-Dimensional Gas of Massless Dirac Fermions in Graphene. *Nat. Phys.* **2005**, *438*, 197–200.
6. Stankovich, S.; Dikin, D. A.; Kohlhaas, K. M.; Zimney, E. J.; Stach, E. A.; Piner, R. D.; Nguyen, S. T.; Ruoff, R. S. Graphene-Based Composite Materials. *Nature* **2006**, *442*, 282–286.
7. Zhang, Y.; Tan, Y.-W.; Stormer, H. L.; Kim, P. Experimental Observation of the Quantum Hall Effect and Berry's Phase in Graphene. *Nature* **2005**, *438*, 201–204.
8. Hernandez, Y.; Nicolosi, V.; Lotya, M.; Blighe, F. M.; Sun, Z.; De, S.; McGovern, I. T.; Holland, B.; Byrne, M.; Gun'Ko, Y. K.; *et al.* High-Yield Production of Graphene by Liquid-Phase Exfoliation of Graphite. *Nat. Nanotechnol.* **2008**, *3*, 563–568.
9. Athanasios, B. B.; Vasilios, G.; Radek, Z.; Theodore, A. S.; Athanasios, K. S. Liquid-Phase Exfoliation of Graphite Towards Solubilized Graphenes. *Small* **2009**, *5*, 1841–1845.
10. Park, H. J.; Meyer, J.; Roth, S.; Skákalová, V. Growth and Properties of Few-Layer Graphene Prepared by Chemical Vapor Deposition. *Carbon* **2010**, *48*, 1088–1094.
11. Weixia, Z.; Jiecheng, C.; Cheng-an, T.; Yiguang, W.; Zhanping, L.; Li, M.; Yuquan, W.; Guangtao, L. A Strategy for Producing Pure Single-Layer Graphene Sheets Based on a Confined Self-Assembly Approach. *Angew. Chem., Int. Ed.* **2009**, *48*, 5864–5868.
12. Li, X.; Cai, W.; An, J.; Kim, S.; Nah, J.; Yang, D.; Piner, R.; Velamakanni, A.; Jung, I.; Tutuc, E.; *et al.* Large-Area Synthesis of High-Quality and Uniform Graphene Films on Copper Foils. *Science* **2009**, *324*, 1312–1314.
13. Li, D.; Muller, M. B.; Gilje, S.; Kaner, R. B.; Wallace, G. G. Processable Aqueous Dispersions of Graphene Nanosheets. *Nature* **2008**, *3*, 101–105.
14. Williams, G.; Seger, B.; Kamat, P. V. TiO_2−Graphene Nanocomposites. UV-Assisted Photocatalytic Reduction of Graphene Oxide. *ACS Nano* **2008**, *2*, 1487–1491.
15. Allen, M. J.; Tung, V. C.; Kaner, R. B. Honeycomb Carbon: A Review of Graphene. *Chem. Rev.* **2010**, *110*, 132–145.
16. Chen, S.; Zhu, J.; Wu, X.; Han, Q.; Wang, X. Graphene Oxide−MnO_2 Nanocomposites for Supercapacitors. *ACS Nano* **2010**, *4*, 2822–2830.
17. Mulvaney, P.; Cooper, R.; Grieser, F. Kinetics of Reductive Dissolution of Colloidal Manganese Dioxide. *J. Phys. Chem.* **1990**, *94*, 8339–8345.
18. Zhang, X.; Wang, Y.; Chen, X.; Yang, W. Fabrication and Characterization of a Novel Inorganic MnO_2/LDHs Multilayer Thin Film *via* a Layer-By-Layer Self-Assembly Method. *Mater. Lett.* **2008**, *62*, 1613–1616.
19. Devaraj, S.; Munichandraiah, N. Effect of Crystallographic Structure of MnO_2 on Its Electrochemical Capacitance Properties. *J. Phys. Chem. C* **2008**, *112*, 4406–4417.
20. Jin, X.; Zhou, W.; Zhang, S.; Chen, G. Z. Nanoscale Microelectrochemical Cells on Carbon Nanotubes. *Small* **2007**, *3*, 1513–1517.
21. Stoller, M. D.; Park, S.; Zhu, Y.; An, J.; Ruoff, R. S. Graphene-Based Ultracapacitors. *Nano Lett.* **2008**, *8*, 3498–3502.
22. Subramanian, V.; Zhu, H.; Vajtai, R.; Ajayan, P. M.; Wei, B. Hydrothermal Synthesis and Pseudocapacitance Properties of MnO_2 Nanostructures. *J. Phys. Chem. B* **2005**, *109*, 20207–20214.
23. Xu, M.; Kong, L.; Zhou, W.; Li, H. Hydrothermal Synthesis and Pseudocapacitance Properties of α-MnO_2 Hollow Spheres and Hollow Urchins. *J. Phys. Chem. C* **2007**, *111*, 19141–19147.
24. Yu, P.; Zhang, X.; Wang, D.; Wang, L.; Ma, Y. Shape-Controlled Synthesis of 3D Hierarchical MnO_2 Nanostructures for Electrochemical Supercapacitors. *Cryst. Growth Des.* **2009**, *9*, 528–533.
25. Kuratani, K.; Tatsumi, K.; Kuriyama, N. Manganese Oxide Nanorod with 2 ×4 Tunnel Structure: Synthesis and Electrochemical Properties. *Cryst. Growth Des.* **2007**, *7*, 1375–1377.